# Generalized Power Flow Analysis of Electrical Power Systems Modeled as Mixed Single-Phase/Three-Phase Sub-Systems

F. Bizzarri, *Senior Member, IEEE*, A. Brambilla *Member, IEEE*,

***Abstract*—Electrical power generation, transmission and distribution systems are often simulated through the single-phase equivalent model by assuming the presence of only the positive sequence in the real system. The well known power flow (PF) analysis is typically used to determine the steady state solution of these single-phase models. After the PF solution was determined, other elements, such as for example synchronous generators and controllers, are initialised. This provides the initial conditions to subsequent transient stability analyses. Nowadays, this simulation approach may be no longer feasible due to the large penetration of unbalanced and/or electronic elements in the power systems. In this paper we present a novel numerical method that allows to freely compute the steady state solution of complex power systems made up of a "mixing" of conventional single-phase models and more complex, detailed three-phase models, for example of some portions of the transmission system and of the distribution ones. This steady state solution can be viewed as a generalization and/or an extension of the conventional PF.**

***Index Terms*—power flow analysis, electromechanical dynamics, electromagnetic dynamics, shooting method.**

## I. Introduction

ELECTRONIC equipments and in particular converters have been more and more used in electric power productions, transmission and distributions systems. Among others, two well known applications are high voltage direct current (HVDC) links where voltage source converters (VSCs) are used to manage the bidirectional power flow from the AC power grid to the DC link and vice versa, and wind farms based on doubly fed induction generators. In both these applications, the converters have complex topologies, may implement sophisticate control algorithms and work at high switching frequencies with respect to the synchronous frequency of the electrical power grid.

In the literature those systems are referred to as hybrid power systems (HPSs) [1]–[5], since they mix what till a few years ago we may had defined as "conventional" and "unconventional" power systems. During the design of these HPSs their numerical analysis is a valid tool to improve reliability, reduce the design cycle, lower the design cost and time. A clear picture of the need of numerical tools able to simulate HPSs is given in [6], [7]. One of the first and largely performed numerical analyses is power flow (PF). The conventional PF is based on a deep exploitation of the single-phase equivalent model of the power system. It assumes that the power system operates in a steady state condition and that only the positive sequence is present. This leads to a solution computed by PF composed of *constant* power levels, voltages and currents in the DQ reference frame.

In the recent past, when designers were dealing with HPSs and there was the need to compute the PF, the fast electromagnetic sub-systems (ESSs) were simplified for example by applying averaging techniques and transformations in the equivalent DQ frame. This was justified since the portion of the power system involving electromagnetic-transients was relatively small and "fast" and it involved a relatively small power level. This paradigm may be no longer acceptable since the electromagnetic dynamic may govern the stability of the entire power system. For example, a very complex control digital algorithm, implemented to enhance the performances on a wind generator in a very large wind farm, can not be conveniently modeled by an equivalent proportional/integral controller as a compromise of the application of some reduction techniques.

All this has triggered the need to develop new simulation tools that should be able to deal with ESSs. For example in [8], the authors propose an approach to enhance the largely used EMTP simulation program to simulate also modular multilevel converters in HVDC links. In [9] power lines can be modeled and simulated as dynamic elements together with the conventional models of the single-phase representation. In [10] a hybrid simulator is proposed that links once more the two different modeling paradigms. In [2], [3] the transmission system is modeled with a three-sequence formulation and the distribution system is modeled with the three-phase formulation. These two representation coexist to perform time domain stability analyses. In [4] an extended three-sequence formulation of the PF problem is provided through the reintroduction of the well known modified nodal analysis [11], [12]. These methods focus on the time domain simulation of hybrid systems and allow the analysis of fault and post-fault phenomena. However these time domain simulations need an initial condition from which to start the analyses. The dynamic parts of the power system such as for example the synchronous generators, automatic voltage regulators, turbine governors, can be initialised only after the PF solution was determined.

To the author knowledge those methods implement simplified algorithms to try to compute the initial condition or even completely neglect the problem of accurately computing the

Federico Bizzarri and Angelo Brambilla are with Politecnico di Milano, DEIB, p.za Leonardo da Vinci, n. 32, I20133 Milano, Italy. E-mail: {federico.bizzarri, angelo.brambilla}@polimi.it

Federico Bizzarri is also with the Advanced Research Center on Electronic Systems "E. De Castro" (ARCES), University of Bologna, Italy.

PF of an HPS, where loads in the distribution system may be unbalanced and/or voltages and currents may be polluted by a high harmonic content (which makes the use of the three-sequence representation inadequate).

In this paper we propose a new approach to perform a generalized PF analysis of HPSs that allows the user to freely build up a complex electrical power system, by mixing conventional single-phase electromechanical models with advanced three-phase electromagnetic ones. We introduce and describe a new simulation paradigm based on a *virtual element* used to interconnect the power electromechanical sub-system (PSS) and the ESS. In the paper this element is referred to as virtual connector (VC). We use the word "virtual" since as shown it is not a real element but something that suitably handles electrical quantities at the interface between the PSS and the ESS. We discuss a global index that suggests whether the choice of insertion of these interfacing VCs is reliable or not.

Another important aspect considered in this paper is the stability analysis of HPSs. The stability analysis of the solution found by conventional PF through the computation of the generalised eigenvalues is a usual numerical practice. We present an innovative and relevant result, i.e., the proposed approach allows us to perform the stability analysis of HPSs through Floquet theory [13]. Two case studies that show the potentiality and effectiveness of the proposed method are presented following a bottom-up approach with respect to complexity. The first case is a simple system that can be solved by "pen and paper" and the second one is the well known IEEE 9-bus 3-generator test system with the addition of a distribution sub-system and a three-phase photovoltaic plant.

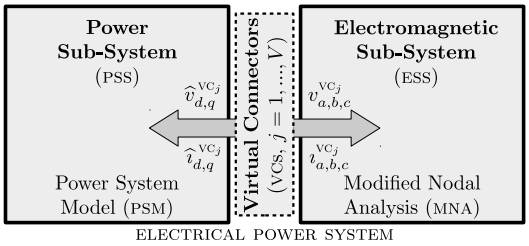


Figure 1. The classical PSM of the PSS and the MNA three-phase model of the ESS communicate through a virtual connector (VC) which *is not an element of the original electrical network to be analysed.*

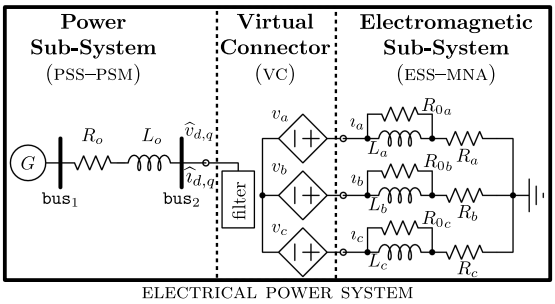


Figure 2. The schematic of the basic mixed electrical system used to exemplify the operating principle of the proposed numerical and modeling approach. Only one VC is used hence $V = 1$, for compactness the $\text{VC}_1$ superscript is dropped. The power generator is the two-axis type 2: $\texttt{vrating} = 100\,\text{kV}$, $\texttt{pgrating} = 100\,\text{MW}$, $\texttt{vg} = 1\,\text{pu}$, $\texttt{ra} = 10^{-3}\,\text{pu}$, $\texttt{m} = 1\,\text{pu}$, $\texttt{d} = 2\,\text{pu}$, $f_o = 50\,\text{Hz}$. Power line: $r = 0$, $x = 0.2\,\text{pu}$. Three-phase balanced load: $R_{0_a,0_b,0_c} = 1\,\text{M}\Omega$, $R_{a,b,c} = 100\,\Omega$, $L_{a,b,c} = 10\,\text{mH}$.

## II. Modeling the overall electrical system

In Fig. 1 a high-level block schematic of an electrical power system is shown. It represents an electrical network split into two distinct parts, the power electromechanical sub-system (PSS) model and the electromagnetic sub-system (ESS) model. The former is described by resorting to the classical power system model (PSM) [14], i.e., to the single-phase equivalent model and the latter through the three-phase dynamic representation. The entire power system exploits the modified nodal analysis (MNA) representation to implement the constitutive equations of elements [11], [12]. To enable the communication between these two sub-systems a VC block is introduced. More than a single VC can be considered if the PSS and the ESS are linked at multiple connection points.

A basic example is presented in Fig. 2. The PSS is composed of a generator, a line and two buses modeled with the single-phase representation in the DQ frame. The $\texttt{bus}_2$ plays an important role since it is at the interface between the PSS and the VC and the interaction takes place by way of the $\widehat{v}_{d,q}$ voltages and the $\widehat{\imath}_{d,q}$ currents. The former can be viewed as the real and imaginary components of the complex voltage at $\texttt{bus}_2$. The latter are the real and imaginary components of the complex currents flowing into the ESS that, thanks to the VC block, can be seen as an equivalent PSM component by the PSS; this is a key aspect. In this case, the ESS is a simple three-phase linear load with the $\imath_{a,b,c}$ currents flowing through it. It is thus modeled as an electric circuit fed by the voltages $v_{a,b,c}$ that are intrinsic variables of the VC. This triplet is the translation of the $\widehat{v}_{d,q}$ voltages available thanks to the VC.

We see also the presence of the filter block that we describe in the sequel.

### A. The power electromechanical sub-system (PSS) model

The PSS model is described through the single-phase equivalent representation. In a formal way the PSM is generically formulated in the DQ-frame by the differential algebraic equation (DAE)

$$\begin{aligned} &\frac{d\widehat{\mathbf{u}}}{dt} + \mathbf{r}\left(\widehat{\mathbf{u}}, \widehat{\mathbf{z}}\right) = 0 \\ &\mathbf{h}\left(\widehat{\mathbf{u}}, \widehat{\mathbf{z}}\right) = 0 \ , \end{aligned} \tag{1}$$

where $\mathbf{r} : \mathbb{R}^{S_u+S_z} \to \mathbb{R}^{S_u}$, $\mathbf{h} : \mathbb{R}^{S_u+S_z} \to \mathbb{R}^{S_z}$, $\widehat{\mathbf{u}} \in \mathbb{R}^{S_u}$ are the state variables (introduced for example by generators, regulator, controllers) spanning the PSS phase space[1], $\widehat{\mathbf{z}} \in \mathbb{R}^{S_z}$ are the algebraic variables (e.g, bus voltages, currents). Equation (1) could explicitly depend on time and involve also discrete variables modeling events, e.g., line outages and faults, switching operation of tap-changers, making it a hybrid dynamical system [15]. Without loss of generality we focus only on autonomous and continuous DAEs. By assuming $V$

[1]The *phase space* is the space in which all possible states of a dynamical system are represented. For a DAE the dimension of the phase space is given by the number of differential variables. In this case such a dimension is $S_u$.

linking points, between the PSS and the ESS, the $V$ subset of the $B$ buses of the PSS plays a special role in the network since each of those is connected (also) to a VC. From a modeling point of view, the equivalent effect of the VCs on these buses is to make them *slack*. *The* VC *forces the voltage of the bus at which it is connected and the current through it is a free variable.* The VCs set $V$ pairs of voltages $\widehat{\boldsymbol{v}}_{d,q}^{\text{VC}} = \left[\widehat{v}_{d,q}^{\text{VC}_1}, \ldots, \widehat{v}_{d,q}^{\text{VC}_V}\right]$ at the corresponding connection buses. The $V$ pairs of $\widehat{\boldsymbol{\imath}}_{d,q}^{\text{VC}} = \left[\widehat{\imath}_{d,q}^{\text{VC}_1}, \ldots, \widehat{\imath}_{d,q}^{\text{VC}_V}\right]$ currents flowing through the VCs from the PSS side appear in the enlarged algebraic-variable vector. Formally, (1) becomes[2]

$$\begin{aligned} &\frac{d\widehat{\mathbf{u}}}{dt} + \mathbf{r}(\widehat{\mathbf{u}}, \overbrace{\left[\widehat{\mathbf{z}}, \widehat{\boldsymbol{\imath}}_{d,q}^{\text{VC}}\right]}^{\widehat{\boldsymbol{\zeta}} \in \mathbb{R}^{S_z+2V}}) = 0 \\ &\mathbf{h}(\widehat{\mathbf{u}}, \widehat{\boldsymbol{\zeta}}) = 0 \ . \end{aligned} \tag{2}$$

Note that, whenever the $j$-th VC is disconnected from the PSS the corresponding pair of currents $\widehat{\imath}_{d,q}^{\text{VC}_j}$ does no longer exist and if the ESS were not a part of the overall power network, (2) would reduce to (1).

### B. The electromagnetic sub-system (ESS) model

The ESS block is implemented by a three-phase model that is generically formulated through the DAE

$$\begin{aligned} &\frac{d\mathbf{q}(\mathbf{x})}{dt} + \mathbf{f}(\mathbf{x}, \mathbf{y}, t) = 0 \\ &\mathbf{g}(\mathbf{x}, \mathbf{y}, t) = 0 \ , \end{aligned} \tag{3}$$

where $\mathbf{y} \in \mathbb{R}^{S_y}$ is the vector of the algebraic variables, $\mathbf{q} : \mathbb{R}^{S_x} \to \mathbb{R}^{S_x}$, $\mathbf{f} : \mathbb{R}^{S_x+S_y+1} \to \mathbb{R}^{S_x}$, $\mathbf{g} : \mathbb{R}^{S_x+S_y+1} \to \mathbb{R}^{S_y}$. The entries of $\mathbf{q}$ are capacitive charges and inductive fluxes and those of $\mathbf{x}$ and $\mathbf{y}$ are ground-referenced node voltages and branch currents. Whenever the ESS is an analog mixed signal circuit it can be modeled as a hybrid dynamical system [16]. Here for the sake of simplicity (3) is presented as a continuous DAE only, but numerical results refer to mixed analog/digital three-phase systems.

The ESS is fed by $V$ VCs through $V$ triplets of voltages $\boldsymbol{v}_{a,b,c}^{\text{VC}} = \left[v_{a,b,c}^{\text{VC}_1}, \ldots, v_{a,b,c}^{\text{VC}_V},\right]$ set by $V$ three-phase controlled voltage sources. An expanded representation of a VC that shows these controlled voltage sources is reported in Fig. 2. These components do not admit voltage basis and consequently, as in the PSS case, the algebraic-variable vector is enlarged with the $V$ triplets of currents $\boldsymbol{\imath}_{a,b,c}^{\text{VC}} = \left[\imath_{a,b,c}^{\text{VC}_1}, \ldots, \imath_{a,b,c}^{\text{VC}_V},\right]$ flowing through them. The $\boldsymbol{v}_{a,b,c}^{\text{VC}}$ voltages are interpreted as inputs incoming from the PSS through the VCs. As a consequence such voltages do not appear in the following generalized formulation of (3)[3]

$$\begin{aligned} &\frac{d\mathbf{q}(\mathbf{x})}{dt} + \mathbf{f}(\mathbf{x}, \overbrace{\left[\mathbf{y}, \boldsymbol{\imath}_{a,b,c}^{\text{VC}}\right]}^{\boldsymbol{\lambda} \in \mathbb{R}^{S_y+3V}}, t) = 0 \\ &\mathbf{g}(\mathbf{x}, \boldsymbol{\lambda}, t) = 0 \ . \end{aligned} \tag{4}$$

As stated above, from a circuit point of view, $\boldsymbol{v}_{a,b,c}^{\text{VC}}$ can be represented as voltage controlled voltage sources. The driving signal of the generic $v_{a,b,c}^{\text{VC}_j}$ voltage source is a function of $\widehat{v}_{d,q}^{\text{VC}_j}$, i.e., the voltage of the power bus to which the $j$-th VC is connected. This dependence is formalized by **Property 3** in Section II-C. Whenever the $j$-th VC is disconnected from the ESS the corresponding triplet of currents $\imath_{a,b,c}^{\text{VC}_j}$ vanishes and if the PSS were not a part of the overall power network, (4) would reduce to the classical MNA of the ESS.

### C. The virtual connector (VC) block

The $j$-th VC block (for $j = 1, ..., V$) links $v_{a,b,c}^{\text{VC}_j}$ and $\widehat{v}_{d,q}^{\text{VC}_j}$, $\imath_{a,b,c}^{\text{VC}_j}$ and $\widehat{\imath}_{d,q}^{\text{VC}_j}$. The peculiar properties of VCs are discussed.

**Property 1**: *Being $\imath_{a,b,c}^{\text{VC}_j}$ the currents of the $j$-th* VC *corresponding to $\imath_{d,q}^{\text{VC}_j}$ in the* DQ*-frame, their zero component is null.*

This is dictated by the fact that the PSM of the PSS is typically developed by assuming that zero components are null. Such property is guaranteed by imposing

$$\begin{bmatrix} \imath_d^{\text{VC}_j} \\ \imath_q^{\text{VC}_j} \\ 0 \end{bmatrix} = \overbrace{\begin{bmatrix} \cos(\omega t)\cos\left(\omega t - \frac{2\pi}{3}\right)\cos\left(\omega t + \frac{2\pi}{3}\right) \\ \sin(\omega t)\sin\left(\omega t - \frac{2\pi}{3}\right)\sin\left(\omega t + \frac{2\pi}{3}\right) \\ 1 \qquad\qquad 1 \qquad\qquad 1 \end{bmatrix}}^{\boldsymbol{\Xi}} \mathbf{s}_j^{\text{T}} \boldsymbol{\lambda} \tag{5}$$

where the $\boldsymbol{\Xi}$ matrix represents the Park transformation that computes the direct, quadrature, and zero axis quantities in a two-axis rotating DQ0 reference frame starting from a three-phase signal in the ABC reference frame [14]. The sub-matrix obtained by removing the last row of $\boldsymbol{\Xi}$ is referred to as $\widehat{\boldsymbol{\Xi}}$. The $\omega$ angular frequency is the fundamental frequency of the overall power system network. The $\mathbf{s}_j \in \mathbb{N}^{3\times(S_y+3V)}$ vector is a selector that has only one entry equal to $\sqrt{2/3}$ per row. These entries select the $\imath_{a,b,c}^{\text{VC}_j}$ currents of the $j$-th VC; the corresponding currents in the DQ-frame are $\imath_{d,q}^{\text{VC}_j}$. Note how the last row of $\boldsymbol{\Xi}$ implements a constraint that forces the zero component of the $\imath_{a,b,c}^{\text{VC}_j}$ currents to be null. This impacts on how the three-phase (controlled) generators of the VC are connected, they must be star connected.

**Property 2**: *Being $\imath_{d,q}^{\text{VC}_j}$ the currents of the $j$-th* VC *in the* DQ*-frame, the* PSS *model is fed by*

$$\begin{aligned} \widehat{\imath}_d^{\text{VC}_j} &= \frac{1}{T}\int_{t_0}^{t_0+T} \imath_d^{\text{VC}_j}(\tau)d\tau \\ \widehat{\imath}_q^{\text{VC}_j} &= \frac{1}{T}\int_{t_0}^{t_0+T} \imath_q^{\text{VC}_j}(\tau)d\tau \ , \end{aligned} \tag{6}$$

*where* $T = {}^{2\pi}/_{\omega}$.

[2]It is worth noticing that (i) the $V$ pairs of $\widehat{v}_{d,q}^{\text{VC}_j}$ voltages do not explicitly appear in (2) since they are interpreted as parameters (voltages are forced to the value of these parameters) and (ii) new symbols should be introduced replacing $\mathbf{r}(\cdot)$ and $\mathbf{h}(\cdot)$, since their definition domain was originally contained in $\mathbb{R}^{S_u+S_z}$ (see (1)) and not in $\mathbb{R}^{S_u+S_z+2V}$, but this is not done to keep notation terse.

[3]New symbols should be introduced replacing $\mathbf{f}(\cdot)$ and $\mathbf{g}(\cdot)$, since their definition domain was originally contained in $\mathbb{R}^{S_x+S_y}$ (see (3)) and not in $\mathbb{R}^{S_x+S_y+3V}$, but this is not done to keep notation terse.

The $\widehat{\imath}_{d,q}^{\mathrm{VC}_j}$ currents are the DC components of $\imath_{d,q}^{\mathrm{VC}_j}$ computed by applying a Shannon filter to them (this filter is highlighted in Fig. 1, more details are in Appendix A) This operation is mandatory since $\imath_{d,q}^{\mathrm{VC}_j}$ may be not the *constant envelope* of a three-phase sinusoidal positive sequence, as it is assumed in the PSM and in some approaches mentioned in the Introduction. In fact, since the ESS block typically contains nonlinear elements and/or imbalances, the frequency spectra of $\imath_{d,q}^{\mathrm{VC}_j}$ are richer than a simple tone at $\omega/2\pi$. This filtering completely removes all the components of the spectrum of the $\imath_{d,q}^{\mathrm{VC}_j}$ but that contributing only the positive sequence to the bus to which the VC is connected. By using the $\widehat{\imath}_{d,q}^{\mathrm{VC}_j}$ filtered component, it is thus guaranteed that, in computing the periodic steady state solution of the overall electrical network, bus voltages and powers at the PSS side are constant. We underline that this filtering action makes the VC a dissipative element, thus it potentially alters the PF solution of the mixed PSS/ESS power system. The very definition of VC suggests that such a component does not necessarily exhibit a "physical meaning"; as a first step it can be simply viewed as a signal-processing block. In fact, its physical meaning is actually hidden in the $\mathcal{P}_{\mathrm{hd}}$ power harmonic distortion index (see Section V-A), which represents the amount of power that cannot be transferred by the VC between the ESS and PSS sides. In other words, when the proposed shooting power flow (SHPF) method has computed the PF solution an index referred to as $\mathcal{P}_{\mathrm{hd}}$ is given that shows the fraction of power dissipated by each VC with respect to the transferred one. It is thus left to the user to improve the overall model of the HPS so that the insertion of each VC at suitable interface points does not alter power transfer, i.e., the VC behaves like a *passive* element.

As stated in the manuscript, $\mathcal{P}_{\mathrm{hd}}$ implicitly reveals whether or not the ESS and the PSS are suitably connected. This means that some parts of the PSS must be moved to the ESS in order to have only harmonic-free currents transferred by each VC from the ESS to the PSS.

**Property 3**: *Being* $\widehat{v}_{d,q}^{\mathrm{VC}_j}$ *the constant voltages at the bus in the* PSS *connected to the* $j$*-th* VC*, the* $v_{a,b,c}^{\mathrm{VC}_j}$ *voltages are derived as* $\left[v_a^{\mathrm{VC}_j},\ v_b^{\mathrm{VC}_j},\ v_c^{\mathrm{VC}_j}\right]^{\mathrm{T}} = \sqrt{\frac{2}{3}}\,\widehat{\boldsymbol{\Xi}}^{\mathrm{T}}\left[\widehat{v}_d^{\mathrm{VC}_j},\ \widehat{v}_q^{\mathrm{VC}_j}\right]^{\mathrm{T}}$

**Property 4**: *Assuming* $\boldsymbol{v}_{a,b,c}^{\mathrm{VC}}$ *known and thus deriving* $\boldsymbol{\lambda}$ *by solving* (4)*, the* $\widehat{\boldsymbol{\imath}}_{d,q}^{\mathrm{VC}}$ *currents that flow in the* PSS *injected by the* VC *are computed through* (5) *and* (6)*.*

## III. Problem formulation and numerical solution

The models introduced in Sec. II are used to formulate the problem we are interested in. The solution is made up of two distinct but interacting contributions: the (conventional) PF solution of the PSS, which is a *constant vector*, and the solution of ESS which are *periodic functions* in the time domain. On one side, having chosen the classical PSM to describe the PSS, its periodic steady state solution is a PF solution, i.e., an equilibrium point in an $S_u$-dimensional subspace. It is worth noticing that this constant PF solution, in the classical PSM aims at representing the envelope of the *actual* system dynamics. In other words, the *periodic steady-state* solution at the fundamental frequency with a *constant* envelope is actually represented as a *constant* PF solution playing the role of a *stationary solution*. From the viewpoint of dynamical systems theory, the consideration above means that the stationary PSM solution is not an *isolated equilibrium* but it is embedded in a *continuum of equilibria* [17]. This is confirmed by an *always null eigenvalue* of the Jacobian matrix of the PSM linearized at any PF solution [18]. All together, the admissible PF solutions represent a one-dimensional manifold in the phase space.

The PF solution of the PSS is derived by imposing the $\dfrac{d\widehat{\mathbf{u}}}{dt} = 0$ condition. This corresponds to compute the solution[4] of the fully algebraic system

$$\begin{aligned} \mathbf{r}(\widehat{\mathbf{u}}, \widehat{\boldsymbol{\zeta}}) &= 0 \\ \mathbf{h}(\widehat{\mathbf{u}}, \widehat{\boldsymbol{\zeta}}) &= 0\ . \end{aligned} \tag{7}$$

As far as the ESS is concerned, its periodic steady state solution is formally expressed as a periodic solution, i.e., a limit cycle in an $S_x$-dimensional subspace. It can be derived by adopting a time-domain shooting method [19], [20], possibly extended to hybrid dynamical systems if the ESS is an analog/digital circuit [16], [21]. Equations (4)–(7) are thus gathered and augmented by the periodicity condition $\mathbf{x}(T + t_0) - \mathbf{x}(t_0) = 0$. The proposed SHPF method grounds on the following strategy: the PSS and the ESS are decoupled by fixing $\widehat{\boldsymbol{v}}_{d,q}^{\mathrm{VC}}$ and consequently $\boldsymbol{v}_{a,b,c}^{\mathrm{VC}}$, as briefly introduced before. The PF solution of the PSS and the periodic steady state solution of the ESS are thus derived independently and in parallel. The residue nonlinear function of the $j$-th VC

$$\rho_{d,q}^{\mathrm{VC}_j}\left(\widehat{\boldsymbol{v}}_{d,q}^{\mathrm{VC}}\right) = \widehat{\imath}_{d,q}^{\mathrm{VC}_j} - \frac{1}{T}\int_{t_0}^{t_0+T} \imath_{d,q}^{\mathrm{VC}_j}(\tau)d\tau \tag{8}$$

is computed for $j = 1, ..., V$. A PF solution of the HPS is found when $\rho_{d,q}^{\mathrm{VC}_j}\left(\widehat{\boldsymbol{v}}_{d,q}^{\mathrm{VC}}\right) = 0$, that is, when the current flowing from the bus to the VC equals the filtered current through the VC (see (6)), that in turn depends on $\boldsymbol{\imath}_{a,b,c}^{\mathrm{VC}}$. We use the iterative Newton method to compute the zeros of (8) that leads to the recursion expression

$$\widehat{\boldsymbol{v}}_{d,q}^{\mathrm{VC}^{k+1}} = \widehat{\boldsymbol{v}}_{d,q}^{\mathrm{VC}^{k}} - \frac{\partial \boldsymbol{\rho}_{d,q}^{\mathrm{VC}^k}}{\partial \widehat{\boldsymbol{v}}_{d,q}^{\mathrm{VC}^k}} \boldsymbol{\rho}_{d,q}^{\mathrm{VC}^k}(\widehat{\boldsymbol{v}}_{d,q}^{\mathrm{VC}^k}) \tag{9}$$

where $k$ is the iteration of the Newton method. The Jacobian matrix is derived by tailoring the method used to perform the stability analysis of the solution that is described in the following section. At each iteration of the Newton method a conventional PF solution of the PSS and a periodic steady state solution of the ESS are computed with the VC buses voltages set at $\widehat{\boldsymbol{v}}_{d,q}^{\mathrm{VC}^k}$.

For the sake of comparison, it is worth mentioning that the method described in [2], which as explicitly stated in [2] is an expansion of the approach firstly described in [22], computes the HPS solution through an iterative map. The iterative map is defined as $\mathbf{x}^{k+1} = \boldsymbol{\Phi}\left(\mathbf{x}^k\right)$, for $k = 0, 1, \ldots$, where $\mathbf{x}^k$ is the solution at iteration $k$. Locally the iteration converges only if the eigenvalues of the Jacobian matrix of $\boldsymbol{\Phi}\left(\mathbf{x}^k\right)$ with respect to $\mathbf{x}^k$ are inside the unit circle in the complex plane. This

[4] Actually (7) is nonlinear and possibly it admits more than a single stable solution.

means that even if the solution of the HPS *exists*, the map may diverge and find no solution. The approach presented in [23] is based on a relaxation iteration that once more can be seen as a map and thus suffers of the same drawback. The paper [24] by the same authors of [23] analyses the convergence issues. We do not use any iterative map to solve (8) but the Newton method that thus does not suffer of this drawback. Furthermore, note that the derivation of the Jacobian matrix in (9) is a key aspect in computing the stability properties of the HPS as better detailed in the next section.

## IV. Stability analysis

The solution of the variational model of a DAE system provides the sensitivity of the state variables and algebraic variables, with respect to the initial conditions and (possibly) a set of parameters [13]. The variational model of the ESS is

$$\begin{aligned}
&\frac{\partial \mathbf{q}}{\partial \mathbf{x}}\frac{d\boldsymbol{\psi}_{xx}}{dt}+\frac{\partial \mathbf{f}}{\partial \mathbf{x}}\boldsymbol{\psi}_{xx}+\frac{\partial \mathbf{f}}{\partial \mathbf{y}}\boldsymbol{\psi}_{yx}+\frac{\partial \mathbf{f}}{\partial \boldsymbol{\imath}^{\mathrm{VC}}_{a,b,c}}\boldsymbol{\psi}_{px}=0\\
&\frac{\partial \mathbf{g}}{\partial \mathbf{x}}\boldsymbol{\psi}_{xx}+\frac{\partial \mathbf{g}}{\partial \mathbf{y}}\boldsymbol{\psi}_{yx}+\frac{\partial \mathbf{g}}{\partial \boldsymbol{\imath}^{\mathrm{VC}}_{a,b,c}}\boldsymbol{\psi}_{px}+\\
&\qquad+\sqrt{\tfrac{2}{3}}\frac{\partial \mathbf{g}}{\partial \boldsymbol{v}^{\mathrm{VC}}_{a,b,c}}(\mathbf{1}_V\otimes\widehat{\boldsymbol{\Xi}}^{\mathrm{T}})\boldsymbol{\psi}_{pu}=0\\
&\boldsymbol{\psi}_{xx}(t_0)=\mathbf{1}_{S_x}\ ,
\end{aligned}\tag{10}$$

where $\boldsymbol{\psi}_{xx}=\dfrac{\partial \mathbf{x}(t)}{\partial \mathbf{x}_0}$, $\boldsymbol{\psi}_{yx}=\dfrac{\partial \mathbf{y}(t)}{\partial \mathbf{x}_0}$, $\boldsymbol{\psi}_{px}=\dfrac{d\boldsymbol{\imath}^{\mathrm{VC}}_{a,b,c}}{\partial \mathbf{x}_0}$ are the unknown matrices that are computed by solving (10), and $\boldsymbol{\psi}_{pu}=\dfrac{d\widehat{\boldsymbol{v}}^{\mathrm{VC}}_{d,q}}{\partial \widehat{\mathbf{u}}_0}$ is the matrix that represents the coupling term, $\mathbf{1}_V$ is the identity matrix of size $V$, $\otimes$ is Kronecker's tensor product that creates a square block diagonal matrix by replicating $V$ times the $\widehat{\boldsymbol{\Xi}}^{\mathrm{T}}$ matrix. The $\widehat{\boldsymbol{\Xi}}^{\mathrm{T}}$ matrix appears only in the second equation of (10) since for simplicity sake we have assumed that the $\boldsymbol{v}^{\mathrm{VC}}_{a,b,c}$ parameters act only on the algebraic equations. $\widehat{\boldsymbol{\Xi}}^{\mathrm{T}}$ accounts for the sensitivity of the $\boldsymbol{v}^{\mathrm{VC}}_{a,b,c}$ ESS voltages with respect to the $\widehat{\boldsymbol{v}}^{\mathrm{VC}}_{d,q}$ ones, i.e., the bus voltages of the PSS. The term that contributes to the Jacobian matrix in (9) can be derived as a by-product of the sensitivity of the $\boldsymbol{\imath}^{\mathrm{VC}}_{a,b,c}$ with respect to the $\widehat{\boldsymbol{v}}^{\mathrm{VC}}_{d,q}$ voltages. The $\boldsymbol{\psi}_{pu}$ term suitably forces the ESS according to the variations of the $\widehat{\mathbf{u}}_{\mathbf{0}}$ initial conditions of the state variables of the PSS.

The system (10) has time varying coefficients. For example the $\dfrac{\partial \boldsymbol{q}}{\partial \boldsymbol{x}}$ and $\dfrac{\partial \boldsymbol{f}}{\partial \boldsymbol{y}}$ matrices have entries that are functions of time. These function are computed along the orbit of the steady state solution obtained at convergence of the SHPF, i.e., along one $T$ working period.

To have an insight, even though not complete, to the stability of the system we briefly introduce the Floquet analysis through an example [13]. Assume that there is not any variation of the voltages of the buses at which the VCs are connected. This means that any $\boldsymbol{\delta}_{\boldsymbol{x}}(t_0)$ perturbation to the $\mathbf{x}_0$ initial condition does not change these bus voltages and that $\boldsymbol{\psi}_{pu}=0$. The bus voltages are thus fixed parameters of (10).

Assume that these $\boldsymbol{\delta}_{\boldsymbol{x}}(t_0)$ small perturbations to $\mathbf{x}_0$ can be considered as additive, i.e., do not modify the periodic orbit of the ESS, that is the matrix of time varying functions in (10) does not vary when we apply the $\boldsymbol{\delta}_{\boldsymbol{x}}(t_0)$ perturbations. We can thus adopt for example the variational model solution $\boldsymbol{\psi}_{xx}(T)$ to compute if $\boldsymbol{\delta}_{\boldsymbol{x}}(t_0)$ vanishes or is amplified. We have $\boldsymbol{\delta}_{\boldsymbol{x}}(T)=\boldsymbol{\psi}_{xx}(T)\boldsymbol{\delta}_{\boldsymbol{x}}(t_0)$ and $\boldsymbol{\delta}_{\boldsymbol{x}}(2T)=\dfrac{\partial \mathbf{x}(2T)}{\partial \mathbf{x}(T)}\boldsymbol{\psi}_{xx}(T)\boldsymbol{\delta}_{\boldsymbol{x}}(t_0)$. Since $\dfrac{\partial \mathbf{x}((k+1)T)}{\partial \mathbf{x}(kT)}=\boldsymbol{\psi}_{xx}(T)$ with $k>0$ and integer and since the solution of the ESS *does not change* when the additive perturbation is applied, we have $\boldsymbol{\delta}_{\boldsymbol{x}}(kT)=\boldsymbol{\psi}^k_{xx}(T)\boldsymbol{\delta}_{\boldsymbol{x}}(0)$. It is immediate to conclude that, if the eigenvalues of $\boldsymbol{\psi}_{xx}(T)$, are inside the unit circle in the complex plane, the system is stable since the $\boldsymbol{\delta}_{\boldsymbol{x}}(kT)$ perturbation vanishes, otherwise it is not since $\boldsymbol{\delta}_{\boldsymbol{x}}(kT)$ grows. In the literature, these eigenvalues are referred to as Floquet multipliers [13]. Note that this conclusion on stability is useless since we completely and deliberately ignored the PSM, i.e., we assumed $\boldsymbol{\psi}_{pu}=0$. In the sequel we describe how the complete stability analysis can be performed.

The main aspect is that the solution of the PSM computed by the SHPF is an operating point and not a periodic orbit. A $T$ periodic solution of the PSM can be obtained by considering that it is driven by a constant $\widehat{\boldsymbol{\imath}}^{\mathrm{VC}}_{d,q}$ current vector and that its solution along the $T$ period can be interpreted as a very simple extension of the constant solution that is obviously also $T$ periodic. Having a constant $T$ periodic orbit we derive the variational model of the PSM in a way similar to what we did for the ESS, obtaining

$$\begin{aligned}
&\frac{d\boldsymbol{\chi}_{uu}}{dt}+\frac{\partial \mathbf{r}}{\partial \widehat{\mathbf{u}}}\boldsymbol{\chi}_{uu}+\frac{\partial \mathbf{r}}{\partial \widehat{\mathbf{z}}}\boldsymbol{\chi}_{zu}+\frac{\partial \mathbf{r}}{\partial \widehat{\boldsymbol{\imath}}^{\mathrm{VC}}_{d,q}}\boldsymbol{\chi}_{pu}=0\\
&\frac{\partial \mathbf{h}}{\partial \widehat{\mathbf{u}}}\boldsymbol{\chi}_{uu}+\frac{\partial \mathbf{h}}{\partial \widehat{\mathbf{z}}}\boldsymbol{\chi}_{zu}+\frac{\partial \mathbf{h}}{\partial \widehat{\boldsymbol{\imath}}^{\mathrm{VC}}_{d,q}}\boldsymbol{\chi}_{pu}+\sqrt{\tfrac{2}{3}}\frac{\partial \mathbf{h}}{\partial \widehat{\boldsymbol{v}}^{\mathrm{VC}}_{d,q}}(\mathbf{1}_V\otimes\widehat{\boldsymbol{\Xi}})\boldsymbol{\chi}_{px}=0\\
&\boldsymbol{\chi}_{uu}(t_0)=\mathbf{1}_{S_u}\ ,
\end{aligned}\tag{11}$$

where $\boldsymbol{\chi}_{uu}=\dfrac{d\widehat{\mathbf{u}}(t)}{d\widehat{\mathbf{u}}_0}$, $\boldsymbol{\chi}_{zu}=\dfrac{d\widehat{\mathbf{z}}(t)}{d\widehat{\mathbf{u}}_0}$, $\boldsymbol{\chi}_{pu}=\dfrac{d\,\widehat{\boldsymbol{\imath}}^{\mathrm{VC}}_{d,q}}{d\widehat{\mathbf{u}}_0}$ are the unknown matrices that are computed by solving (11), and $\boldsymbol{\chi}_{px}=\dfrac{d\boldsymbol{\imath}^{\mathrm{VC}}_{a,b,c}}{\partial \widehat{\mathbf{u}}_0}$ is the matrix that represents the coupling term. The structure of (11) is very similar to (10), but there are some differences. The system is forced by a possibly time varying $\boldsymbol{\chi}_{px}$ term. The system has constant coefficient matrices. We underline that in writing (11) we *have not low pass filtered the* $\boldsymbol{\imath}^{\mathrm{VC}}_{q,d}$ *currents* (**Property 2**). This choice was made since in the ideal case the insertion of the VCs in the circuit to link the PSS and ESS sub-systems has to be done in sections that lead only to positive sequences in the PSS, as previously detailed. The harmonics at higher frequencies must give a very limited contribution to preserve the accuracy of the PSS model.

By solving the joined (10) and (11) variational systems and eliminating the $\boldsymbol{\psi}_{pu}$ and $\boldsymbol{\chi}_{px}$ sensitivities, we can finally have

$$\boldsymbol{\Psi}(T)=\begin{bmatrix}\boldsymbol{\psi}_{xx}(T) & \boldsymbol{\psi}_{xu}(T)\\ \boldsymbol{\chi}_{px}(T) & \boldsymbol{\chi}_{pp}(T)\end{bmatrix}\ ,\tag{12}$$

where $\boldsymbol{\Psi}(T)\in\mathbb{R}^{(S_u+2V)\times(S_u+2V)}$ is the sensitivity matrix that shows how the state variables in the PSS and ESS sub-systems vary after one $T$ working period if their values at the beginning of the period are varied by $\boldsymbol{\delta}_{\boldsymbol{x}}(t_0)$ and $\boldsymbol{\delta}_{\boldsymbol{u}}(t_0)$ respectively. The $\boldsymbol{\delta}_{\boldsymbol{u}}\in\mathbb{R}^{S_u}$ is the perturbation vector that

acts on the $\mathbf{u}(t_0)$ initial conditions of the state variables of the PSS sub-system. The eigenvalues of $\mathbf{\Psi}(T)$ are the Floquet multipliers of the full HPS and if they are inside the unit circle in the complex plane the system is stable.

Note that we expect to have a Floquet multiplier (say for example $\lambda_1$) equal to 1, thus exactly on the edge between the stability and instability regions. This means that any perturbation directed as its corresponding eigenvector does not attenuate. This is perfectly coherent with the null eigenvalue that one always finds in the conventional stability analysis performed on the conventional PF solution. This means that the power system does not have any phase reference, the introduction of the slack generator gives a "virtual" phase reference. The null eigenvalue by the stability analysis of the conventional PF analysis corresponds to $\lambda_1 = 1$ [25].

## V. Numerical results

In this section we present two applications of the proposed SHPF method that was implemented in our simulator PAN [26], [27]. Our target is to clearly show the potentiality and effectiveness of SHPF.

The simulations run on a $3.2\,\mathrm{GHz}$–$16\,\mathrm{GByte}$ INTEL-I7 computer running LINUX-MINT-17. In the considered case studies, the SHPF algorithm found a solution in no more than 3 iterations of the Newton method (9). Both the solver that computes the partial solution of the PSS at each iteration of SHPF and the shooting method used to compute the partial solution of the ESS converged in no more that 3 iterations.

We start by considering the very simple linear circuit shown in Fig. 2, which in principle can be solved by "pen and paper". In this case, the dynamics of the load, modelled as a constant impedance in the single-phase equivalent representation, is modeled by the inductors in the three-phase representation. We thus propose something similar to what is done in [9].

The second example is much more complex and is composed of the modified version of the IEEE 9-bus 3-generator power test system shown in Fig. 3.

### A. How much power is dissipated by the VCs

For both the test circuits we compute the $\mathcal{P}^j_{\mathrm{hd}}$ power harmonic distortion of each $j$-th VC. We compute the complex Fast-Fourier transform of the voltages of all the VCs organised in the $\widetilde{v}_j = \left(v^{\mathrm{VC}}_{d,j}, v^{\mathrm{VC}}_{q,j}\mathrm{I}\right) \in \mathbb{C}$ vector, $\mathrm{I} = \sqrt{-1}$ and $j = 1, \ldots, V$, (currents are organised in the same way) and defined

$$\mathcal{P}^j_{\mathrm{hd}} = \frac{\sum_{k=1}^{K} \widetilde{V}_j \widetilde{I}^*_j}{\sum_{k=0}^{K} \widetilde{V}_j \widetilde{I}^*_j} \ ,$$

where the upper case symbols refer to the components of the spectra, $k = 0$ indexes the DC component and $K/2$ is the maximum harmonic in the spectrum (bilateral). The $j$-th $0 \leq \mathcal{P}^j_{\mathrm{hd}} \leq 1$ gives an idea on how much power lays at the other components of the spectrum excluding the DC, that gives the magnitude of the positive sequence.

### B. The very simple example

By referring to the power system in Fig. 2, the models of the power generator and line used in the PSS are those from the user manual of the PSAT simulator [28]; the parameters are reported in the caption of Fig. 2.

The SHPF method computes the $P = 8.227\,\mathrm{MW}$ active and $Q = 27.465\,\mathrm{MVAR}$ reactive power of the synchronous machine. In this example we have that the unique VC is characterised by $\mathcal{P}_{\mathrm{hd}} = 0.000$, showing that the conversion of the electrical quantities from the ESS sub-system to the PSS one generates only the positive sequence, as expected.

The power generator model contributes three state variables[5]. The three inductors "almost" introduce a degeneration that is avoided with the connection in parallel of the corresponding $R_{0_a,0_b,0_c}$ resistors. This leads to a Floquet multiplier with almost null magnitude. Stability analysis correctly provides five significant Floquet multipliers, i.e., $\lambda_1 = 1$, $\lambda_2 = 0.980$, $\lambda_3 = 0.963$ and $\lambda_{4,5} = (0.124 \pm 0.052\,\mathrm{I})$. All the Floquet multipliers, excluding $\lambda_1$ are inside the unit circle in the complex plane and thus the mixed PSS/ESS system is stable, as expected. The $\lambda_1 = 1$ Floquet multiplier corresponds to the null eigenvalue of the stability analysis performed at the solution found by the conventional PF.

We also computed the PF when the power system in Fig. 2 is unbalanced by removing $R_{0_c}$ (open circuit). The SHPF method computes the $P = 4.348\,\mathrm{MW}$ active and $Q = 14.083\,\mathrm{MVAR}$ reactive power of the synchronous machine. The VC blocks the negative and zero sequences from the ESS. This is clearly shown by $\mathcal{P}_{\mathrm{hd}}$ that jumps at $66\%$. This high value of the index clearly shows that the computed PF is not reliable, viz. the basic assumption of injecting only the positive sequence in the PSS is not feasible as expected.

### C. The modified IEEE 9-bus 3-generator test system

In Fig. 3 we show the schematic of the modified version of the IEEE 9-bus 3-generator test system (WECC9B3G). Modification consists in the connection at $\mathtt{bus}_5$ (through a VC) of the three-phase distribution sub-system enclosed in the (blue colored) dashed box. The complete system is composed of the 3 sub-systems shown in Figs. 3, 4 and 5. More details on each sub-system and its parameters can be found in the figure captions. The interested reader may replicate our simulations with different tools or perform time domain analyses to check stability. We considered a non-linear magnetisation inductance of transformers, its characteristic is given in the caption of Fig. 3. The additional $\beta\imath_{\mathrm{a,b,c}}$ (amethyst colored) block magnifies the three-phase $\imath_{\mathrm{a,b,c}}$ current. Thus the current injected in the $\mathtt{b}_1$ bus is $(\beta + 1)\imath_{\mathrm{a,b,c}}$. In this way we replicate several identical distribution systems connected to the same $\mathtt{b}_1$ bus.

At the $\mathtt{b}_4$ (blue colored) bus we connect a three-phase LCL-VSC whose block schematic is shown in Fig. 4. We use a detailed model of the VSC that comprehends the PWM-modulator,

[5]The instantaneous phase of the generator is represented as a periodic function in the Cartesian frame and not as an unbounded function in polar coordinates. The Cartesian frame introduces two state variables to model phase [25].

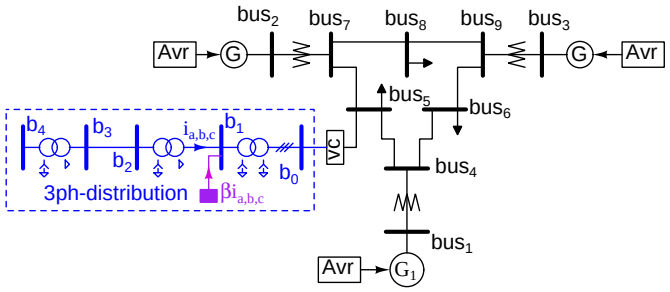


Figure 3. The schematic of the IEEE 9-bus 3-generator test system. The circuit in the (blue colored) dashed box is the three-phase model of a distribution system. The VC connects the $\mathtt{b}_0$ (three-phase) and $\mathtt{bus}_5$ (single-phase) buses. The $\mathtt{b}_1$, $\mathtt{b}_2$, $\mathtt{b}_3$ and $\mathtt{b}_4$ three-phase buses have a voltage rating of 69 kV, 13.8 kV, 13.8 kV and 380 V, respectively. The synchronous frequency is 50 Hz. Three-phase line connecting the $\mathtt{b}_2$, $\mathtt{b}_3$ buses: $X/R$ ratio 20, voltage factor 8%. The model of the transformers is that of the EMTP-RV simulator; impedance voltage drop 14%, ohmic voltage drop 0.5% for all transformers. Magnetizing inductance $L_{\mathrm{mag}} = L_m - 0.999 L_m \tanh(\gamma_s (|\imath_{\mathrm{mag}}| - I_s)$, where $L_m$ is half the inductance in the linear region and $I_s$ is the current at which saturation begins.

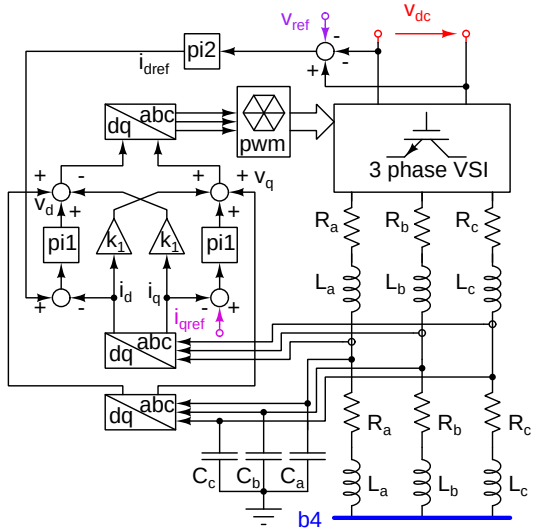


Figure 4. The block schematic of the LCL VSC. $f_{\mathrm{pwm}} = 213 \times 50$ Hz, $L_{a,b,c} = 1.8$ mH, $R_{a,b,c} = 100$ mΩ, $C_{a,b,c} = 27$ µF, $k_{i1} = 20$, $k_{p1} = 50$, $k_1 = 100\pi L_{a,b,c}$, $k_{i2} = 20$, $k_{p2} = 50$, $\imath_{\mathrm{qref}} = 0$.

the three-phase switching legs (IGBTs, diode snubbers) and the controller. The gate signals of the IGBTs are generated by the pwm digital block; it is implemented through the VERILOGA-RTL formal language. Thus the SHPF method finds the solution of a mixed analog/digital circuit. The pi2 proportional-integral (PI) control block senses the $\mathrm{v}_{\mathrm{dc}}$ input voltage of the VSC and acts on the $\imath_{\mathrm{dref}}$ signal so that $\mathrm{v}_{\mathrm{dc}}$ is kept at $\mathrm{v}_{\mathrm{ref}}$.

The DC input of the VSC is connected to the output of the DC/DC converter shown in Fig. 5, that transfers power from the pv array of solar panels. The DC/DC converter is equipped with a perturb and observe (P&O) maximum power point tracker (MPPT) [29]. The MPPT senses the instantaneous power delivered by pv with a period of 5 ms and varies the $\mathrm{v}_{\mathrm{ref}}$ reference voltage by a discrete step to obtain the maximum power generation from pv. The duty-cycle of $\mathrm{Q}_1$ is varied in

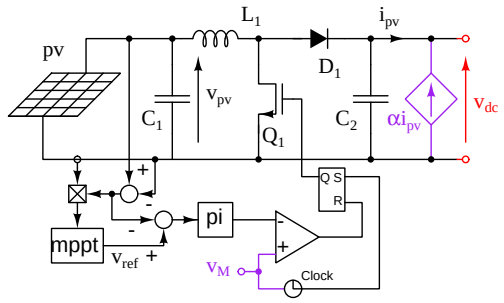


Figure 5. The block schematic DC/DC converter. $C_1 = 10$ µF, $C_2 = 100$ µF, $L_1 = 138$ µH. $k_{i1} = 0.5$, $k_{p1} = 0.5$, $f_{\mathrm{pwm}} = 2 \times 213 \times 50$ Hz, saw-tooth waveform between 0 V and 3 V. The model of the pv array of solar panels can be found in the manual of PSIM. It is composed of 360 cells connected in series. Solar radiation 1 kWm$^{-2}$, pv working temperature 50 °C.

order to set the $\mathrm{v}_{\mathrm{pv}}$ voltage at $\mathrm{v}_{\mathrm{ref}}$, i.e., to meet the maximum power transfer condition. The $\mathrm{v}_{\mathrm{M}}$ input of the DC/DC converter is the PWM signal. At each falling edge of this signal the FLIP-FLOP is set and $\mathrm{Q}_1$ is turned on. The comparator resets the gate signal when the PWM ramp crosses the output of the pi block. Once more the comparator and the FLIP-FLOP are implemented with the VERILOGA-RTL language. The (amethyst colored) current controlled current source emulates the connection in parallel of several DC/DC converters (i.e., of several strings of pvs) by magnifying by $\alpha$ the $\imath_{\mathrm{pv}}$ current.

We are interested in computing the PF solution of the entire power system through the proposed SHPF method. We underline that the PF solution depends on the efficiency of the converters, on the behaviour of the MPPT, on the solar radiation and working temperature of the pv array of solar panels and on the characteristics of the distribution system. We compute the PF solution at different levels of the $S$ solar irradiance (200 Wm$^{-2}$, 1 kWm$^{-2}$ and 1.15kWm$^{-2}$). Being the MPPT a P&O type, the power generated by the pv periodically varies in one period of the 50 Hz synchronous frequency. For example, this is shown in Fig. 6(b) that reports the instantaneous power at the output of the DC/DC converter.

The PF computed by the SHPF can be organised in two parts: one refers to the PSS sub-system and is composed of constant values and the other refers to the ESS and is composed of periodic functions with period $T = 1/50$. Some constant entries of the PSS sub-system solution are reported in Table I. In particular we report the active/reactive powers of the three

Table I
PSS SOLUTIONS WITH DIFFERENT VALUES OF THE $S$ IRRADIANCE.

| $S$ | 200 | 1000 | 1150 |
|---|---|---|---|
| $P_{\mathrm{G}_1}$ | 69.884 | 62.381 | 60.986 |
| $Q_{\mathrm{G}_1}$ | 22.338 | 21.778 | 21.693 |
| $Q_{\mathrm{G}_2}$ | 3.819 | 3.480 | 3.425 |
| $Q_{\mathrm{G}_3}$ | −12.220 | −12.328 | −12.343 |
| $v_{d,q}^{\mathrm{bus}_5}$ | (230.06, −15.54) | (230.40, −13.37) | (230.46, −12.96) |
| $\mathcal{P}_{\mathrm{hd}}$ | 0.20% | 0.26% | 0.37% |

Irradiance is expressed in Wm$^{-2}$; active and reactive powers are in MW and MVAR, respectively; (d,q) voltages are in kV.

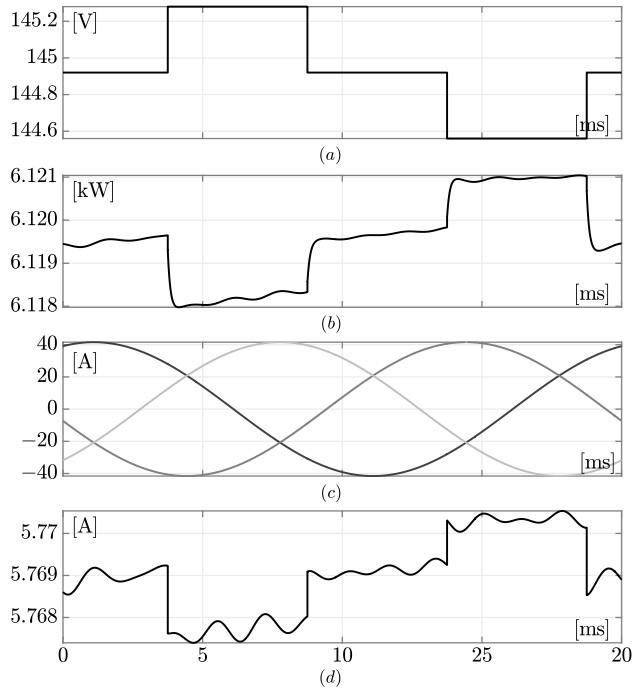


Figure 6. $S = 1000\,\mathrm{Wm}^{-2}$. (a) $\mathrm{v_{ref}}$ voltage determined by the MPPT, y-axis: voltage [V]. (b) The instantaneous power at the output of the DC/DC converter, y-axis: power [kW]. (c) The $\imath_{a,b,c}$ three-phase currents of the VC in Fig. 3, (d) The $\imath_{dref}$ driving signal of the LCL converter. y-axis: current [A]. x-axes: time [ms].

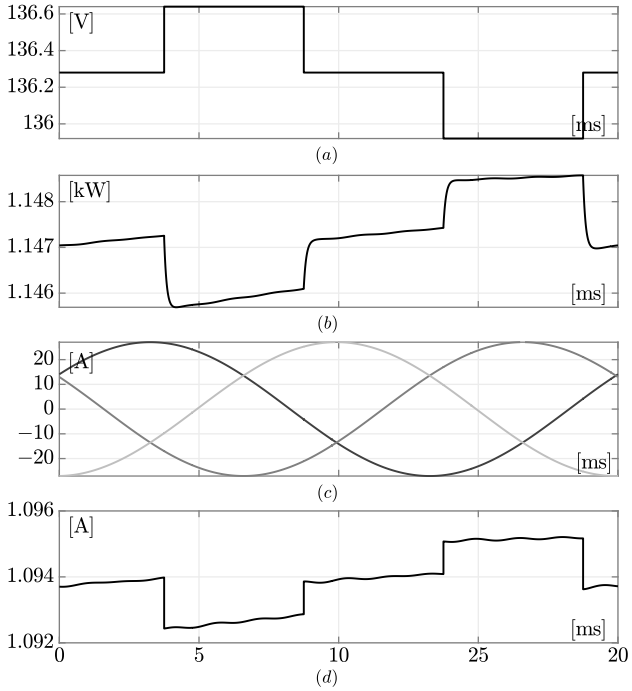


Figure 7. $S = 200\,\mathrm{Wm}^{-2}$. (a) $\mathrm{v_{ref}}$ voltage determined by the MPPT, y-axis: voltage [V]. (b) The instantaneous power at the output of the DC/DC converter, y-axis: power [kW]. (c) The $\imath_{a,b,c}$ three-phase currents of the VC in Fig. 3, (d) The $\imath_{dref}$ driving signal of the LCL converter. y-axis: current [A]. x-axes: time [ms].

synchronous generators, the voltage at $\mathrm{bus}_5$ and the $\mathcal{P}_{\mathrm{hd}}$ index.

Fig. 6 refers to the $S = 1000\,\mathrm{Wm}^{-2}$ case, i.e., the nominal irradiance. Due to the low value of $\mathcal{P}_{\mathrm{hd}}$, the $\imath_{a,b,c}$ three-phase periodic currents of the unique VC appear as perfectly sinusoidal. The low value of $\mathcal{P}_{\mathrm{hd}}$ shows that the accuracy of the obtained PF is largely acceptable since if the filter of the VC would be removed, the Park transform would basically inject only the positive sequence in the PSS, which is the optimal situation since the VC behaves like a passive element. In Fig. 6 we show also the periodic $\mathrm{v_{ref}}$ by the MPPT.

The stability analysis shows that the first three eigenvalues with largest modulus of (12), i.e., the first three Floquet multipliers, are $\lambda_1 = 1.00$, $\lambda_2 = 0.98 \pm 0.15\mathrm{I}$ and $\lambda_3 = 0.99$. They are inside the unit circle in the complex plane and thus the PF solution is stable.

For comparison we report the PF solution of the conventional WECC9B3G, i.e., without the addition of the distribution system, $P_{\mathrm{G_1}} = 71.641\,\mathrm{MW}$, $Q_{\mathrm{G_1}} = 27.046\,\mathrm{MVAR}$, $v_{d,q}^{\mathrm{bus_5}} = (228.44, -15.39)\,\mathrm{kV}$. The reactive powers of the other two PV generators are $Q_{\mathrm{G_2}} = 6.653\,\mathrm{MVAR}$ and $Q_{\mathrm{G_3}} = -10.860\,\mathrm{MVAR}$ The active and reactive power of $\mathrm{G_1}$ is higher due to the lack of power generation by the photovoltaic plant.

The same type of waveforms shown in Fig. 6 are reported in Fig. 7 for the $S = 200\,\mathrm{Wm}^{-2}$ case. We see that the MPPT sets the working point at a lower voltage (about 136 V instead of 145 V of the previous case), that the input power of the LCL converter is less and that consistently the magnitude of the $\imath_{a,b,c}$ currents of the VC is less. One relevant aspect is that the $\mathrm{i_{dref}}$ control signal of the LCL VSC converter shown in Fig. 4 is less undulatory than in the $S = 1000\,\mathrm{Wm}^{-2}$ case. In Fig. 8 we report the same waveforms of the previous cases with $S = 1150\,\mathrm{Wm}^{-2}$. We see that the undulations of $\mathrm{i_{dref}}$ are further increased with respect to the $S = 1000\,\mathrm{Wm}^{-2}$ case. This reflects also the $\mathcal{P}_{\mathrm{hd}}$ values shown in Table I.

We underline that this analysis of the WECC9B3G hybrid test system used as demonstration vehicle were performed in a few tens of seconds of CPU time by allowing a straightforward use of mixed models.

As far as we know, the comparison of the results by SHPF with those by other simulation tools is not an easy task due to the novelty of the method. We tried to mitigate this aspect by performing some cross checks between the solutions computed by the conventional PF and SHPF. Firstly we performed a conventional PF with the distribution sub-system replaced by an equivalent PQ load. The power values are those of the VC in Fig. 3 computed by the SHPF with $S = 1000\,\mathrm{Wm}^{-2}$, i.e., $P_{\mathrm{vc}} = -9.13\,\mathrm{MW}$, $Q_{\mathrm{vc}} = -7.39\,\mathrm{MVAR}$. The conventional stability analysis shows that $\mu_1 = -0.0631$ is the largest eigenvalue, neglecting that equal to 0, i.e., the power system is stable. This result is coherent with that by Floquet analysis, i.e., all but one multiplier are inside the unit circle in the complex plane. Then, we did the opposite. We know that the WECC9B3G is unstable if the automatic voltage regulators are removed. In this case the conventional PF computes an eigenvalue equal to $\mu_1 = 0.0479$ (positive). We repeated the same simulation with the full system by SHPF and obtained the largest Floquet multiplier is $\lambda_1 = 1.0010$, which shows

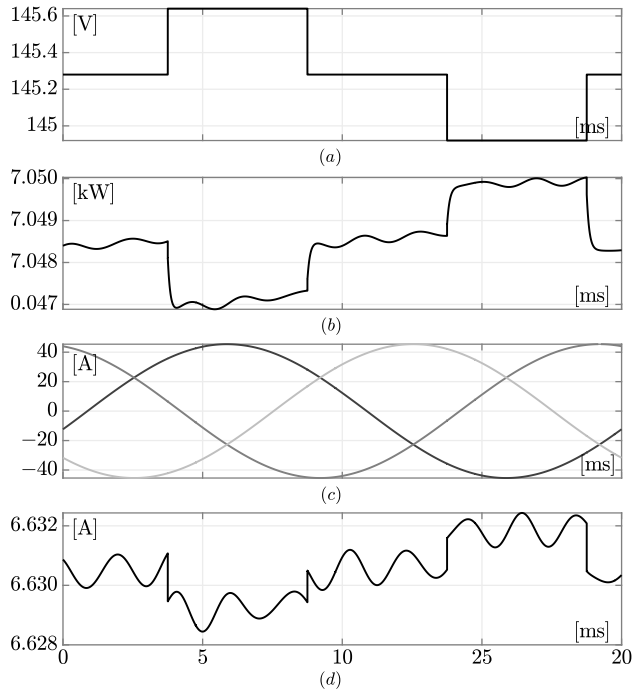


Figure 8. $S = 1150\,\mathrm{Wm}^{-2}$. (a) $\mathrm{v_{ref}}$ voltage determined by the MPPT, y-axis: voltage [V]. (b) The instantaneous power at the output of the DC/DC converter, y-axis: power [kW]. (c) The $\imath_{a,b,c}$ three-phase currents of the VC in Fig. 3, (d) The $\imath_{dref}$ driving signal of the LCL converter. y-axis: current [A]. x-axes: time [ms].

instability. Note that in this case we have $\lambda_1 = e^{\mu_1/f_o}$.

A different scenario can be obtained by altering the magnitude of the bus voltages of the PSS by acting for example on the parameters of the AVR, and/or transformers. In particular if the nominal magnitude of the $\mathtt{bus_5}$ voltage is lowered by $10\%$ the HPS becomes unstable. In this case we have the PF solution: $P_{\mathrm{G}_1} = 63.710\,\mathrm{MW}$, $Q_{\mathrm{G}_1} = 35.883\,\mathrm{MVAR}$, $Q_{\mathrm{G}_2} = 20.333\,\mathrm{MVAR}$, $Q_{\mathrm{G}_3} = 1.7584\,\mathrm{MVAR}$ and $v_{d,q}^{\mathrm{bus}_5} = (202.13, -15.036)\,\mathrm{kV}$. The Floquet multipliers with largest modulus are the complex conjugated pair $\lambda_{1,2} = 0.35 \pm 0.99\mathrm{I}$ that falls outside the unit circle in the complex plane being $|\lambda_{1,2}| = 1.05$. This shows that the overall power system modeled as an HPS is unstable. A time domain analysis started from the initial conditions computed by the SHPF confirms that the HPS is unstable.
The other methods mentioned in this paper do not present any stability analysis and this results can be obtained only by considering the full dynamics property of the ESS and its periodic solution together with sensitivity matrices. Moreover, if Thévenin or Norton equivalents were used for the ESS they would *destroy* its dynamics thus preventing the possibility to perform any overall stability analysis.

## VI. Conclusions

We have described an algorithm to compute the steady state solution of power systems modeled as a mix of conventional single-phase equivalents and three-phase detailed dynamic models interfaced by virtual connectors (VCs). We obtain a generalized PF solution of the overall system, that we refer to as SHPF solution since it is achieved through cooperating conventional PF analysis and shooting time-domain method. We underline that such a SHPF solution consists of a steady state periodic orbit at the three-phase side and of a constant solution at the single-phase equivalent side.
Furthermore the proposed approach provides a global index that suggests whether the choice of insertion of these interfacing VCs is reliable or not.

The target of this method is to give a correct initial condition for the subsequent time domain stability analysis of the hybrid power system, i.e., it allows us to correctly initialise the dynamic elements of the single-phase equivalent model such as for example synchronous generators, shaft models, voltage regulators, turbine governors. A subsequent time domain stability analysis of the hybrid power system can be started from the equilibrium point of the PSS (dynamic elements included) and from the desired point of the periodic solution of the ESS.

Furthermore the proposed method allows to freely build the hybrid system without resorting to simplifications such as for example averaging techniques to derive single-phase compatible models.

The main drawback of the proposed method is that the detailed models of three-phase switching sub-circuits, such as for example the DC/DC and the LCL-VSC of the reported example, must have a working period that is equal to $^{n}/_{(mf_o)}$ where $f_o$ is the synchronous frequency, $n$ and $m$ are integers (better if small to perform simulations in a reasonable CPU time). This is due to a well known drawback of the shooting method used to solve the detailed three-phase sub-system.

In the near future we plan to develop an efficient method to simulate the mixed/hybrid power systems in the time domain to study stability and fault and post-fault effects. We will use the proposed SHPF solution to compute the initial conditions of the overall system.

## Appendix

The Shannon filter implements a low-pass filter with rectangular frequency mask. Components of the frequency spectrum falling outside this mask are perfectly filtered out. If the $x(t)$ time domain signal at the output of the filter is sampled at fixed time intervals at least twice the frequency of the Shannon filter bandwidth, the time domain waveform can be exactly reconstructed from these samples through the Whittaker–Shannon interpolation formula

$$x(t) = \sum_{n=-\infty}^{\infty} x(nT)\mathrm{sinc}\left(\frac{t-nT}{T}\right) ,$$

where $x(nT)$ are the samples, $T = {}^{1}/_{(2f_{\mathrm{bw}})}$ is the sampling time interval with $f_{\mathrm{bw}}$ the bandwidth of the Shannon filter and $\mathrm{sinc}()$ is the sinc function [30]. The Shannon filter is non-causal but this is not a problem since we solve the ESS with the shooting method and thus we compute the solution along a full working period and at an even time mesh. The application of the Shannon filter allows us to accurately perform the numerical computation of the $\widehat{\imath}_{d,q}$ currents and of the $\mathcal{P}_{\mathrm{hd}}$ index.

## REFERENCES


[1] J. Jardim, K. Salim, P. Santos, C. Neto, M. Santos, H. Barros, and G. Taranto, "Variable time step application on hybrid eletromechanical-eletromagnetic simulation," *IET Generation, Transmission Distribution*, vol. 11, no. 12, pp. 2968–2973, 2017.

[2] Q. Huang and V. Vittal, "Integrated transmission and distribution system power flow and dynamic simulation using mixed three-sequence/three-phase modeling," *IEEE Trans. on Power Systems*, vol. 32, no. 5, pp. 3704–3714, Sept 2017.

[3] ——, "Advanced emt and phasor-domain hybrid simulation with simulation mode switching capability for transmission and distribution systems," *IEEE Trans. on Power Systems*, vol. 33, no. 6, pp. 6298–6308, Nov 2018.

[4] I. Kocar, J. Mahseredjian, U. Karaagac, G. Soykan, and O. Saad, "Multiphase load-flow solution for large-scale distribution systems using mana," in *2014 IEEE PES General Meeting — Conference Exposition*, July 2014, pp. 1–1.

[5] D. Shu, X. Xie, Q. Jiang, Q. Huang, and C. Zhang, "A novel interfacing technique for distributed hybrid simulations combining emt and transient stability models," *IEEE Transactions on Power Delivery*, vol. 33, no. 1, pp. 130–140, Feb 2018.

[6] V. Jalili-Marandi, V. Dinavahi, K. Strunz, J. A. Martinez, and A. Ramirez, "Interfacing techniques for transient stability and electromagnetic transient programs ieee task force on interfacing techniques for simulation tools," *IEEE Transactions on Power Delivery*, vol. 24, no. 4, pp. 2385–2395, Oct 2009.

[7] Y. Zhang, A. M. Gole, W. Wu, B. Zhang, and H. Sun, "Development and analysis of applicability of a hybrid transient simulation platform combining tsa and emt elements," *IEEE Transactions on Power Systems*, vol. 28, no. 1, pp. 357–366, Feb 2013.

[8] X. Meng and L. Wang, "Interfacing an emt-type modular multilevel converter hvdc model in transient stability simulation," *IET Generation, Transmission Distribution*, vol. 11, no. 12, pp. 3002–3008, 2017.

[9] P. Le-Huy, G. Sybille, P. Giroux, L. Loud, J. Huang, and I. Kamwa, "Real-time electromagnetic transient and transient stability co-simulation based on hybrid line modelling," *IET Generation, Transmission Distribution*, vol. 11, no. 12, pp. 2983–2990, 2017.

[10] K. Mudunkotuwa, S. Filizadeh, and U. Annakkage, "Development of a hybrid simulator by interfacing dynamic phasors with electromagnetic transient simulation," *IET Generation, Transmission Distribution*, vol. 11, no. 12, pp. 2991–3001, 2017.

[11] L. Chua, C. A. Desoer, and E. S. Kuh, *Linear and Nonlinear Circuits*. New York: McGraw-Hill, Editions, 1987.

[12] J. Vlach and K. Singhal, *Computer Methods for Circuit Analysis and Design*. Van Nostrand Reinhold Company, 1983.

[13] M. Farkas, *Periodic motions*. New York, NY, USA: Springer-Verlag New York, Inc., 1994.

[14] P. Kundur, N. Balu, and M. Lauby, *Power system stability and control*, ser. EPRI power system engineering series. McGraw-Hill, 1994.

[15] I. A. Hiskens, "Power system modeling for inverse problems," *IEEE Trans. on Circuits and Systems I: Regular Papers*, vol. 51, no. 3, pp. 539–551, March 2004.

[16] F. Bizzarri, A. Brambilla, and G. Storti Gajani, "Steady state computation and noise analysis of analog mixed signal circuits," *Circuits and Systems I: Regular Papers, IEEE Trans. on*, vol. 59, no. 3, pp. 541 –554, March 2012.

[17] B. Aulbach, *Continuous and Discrete Dynamics Near Manifolds of Equilibria*, ser. Lecture Notes in Mathematics. Springer-Verlag, 1984.

[18] P. Sauer and M. A. Pai, "Power system steady-state stability and the load-flow jacobian," *Power Systems, IEEE Trans. on*, vol. 5, no. 4, pp. 1374–1383, Nov 1990.

[19] T. Aprille and T. Trick, "Steady-state analysis of nonlinear circuits with periodic inputs," *Proc. of the IEEE*, vol. 60, pp. 108–114, Jul. 1972.

[20] ——, "A computer algorithm to determine the steady-state response of nonlinear oscillators," *IEEE Transactions on Circuit Theory*, vol. 19, no. 4, pp. 354–360, July 1972.

[21] F. Bizzarri, A. Brambilla, and G. S. Gajani, "Extension of the variational equation to analog/digital circuits: numerical and experimental validation," *International Journal of Circuit Theory and Applications*, vol. 41, no. 7, pp. 743–752, 2012.

[22] H. Sun, Q. Guo, B. Zhang, Y. Guo, Z. Li, and J. Wang, "Master–slave-splitting based distributed global power flow method for integrated transmission and distribution analysis," *IEEE Transactions on Smart Grid*, vol. 6, no. 3, pp. 1484–1492, May 2015.

[23] F. J. Plumier, P. Aristidou, C. Geuzaine, and T. Van Cutsem, "A relaxation scheme to combine phasor-mode and electromagnetic transients simulations," in *2014 Power Systems Computation Conference*, Aug 2014, pp. 1–7.

[24] F. J. Plumier, C. Geuzaine, and T. Van Cutsem, "On the convergence of relaxation schemes to couple phasor-mode and electromagnetic transients simulations," in *2014 IEEE PES General Meeting — Conference Exposition*, July 2014, pp. 1–5.

[25] F. Bizzarri, A. Brambilla, and F. Milano, "The probe-insertion technique for the detection of limit cycles in power systems," *IEEE Trans. on Circuits and Systems I: Regular Papers*, vol. 63, no. 2, pp. 312–321, Feb 2016.

[26] F. Bizzarri and A. Brambilla, "PAN and MPanSuite: Simulation vehicles towards the analysis and design of heterogeneous mixed electrical systems," in *IEEE International Conference of New Generation of Circuits and Systems (NGCAS)*, Sept 2017, pp. 1–4.

[27] F. Bizzarri, A. Brambilla, G. Storti Gajani, and S. Banerjee, "Simulation of real world circuits: Extending conventional analysis methods to circuits described by heterogeneous languages," *IEEE Circuits and Systems Magazine*, vol. 14, no. 4, pp. 51–70, 2014.

[28] F. Milano, "An open source power system analysis toolbox," *Power Systems, IEEE Trans. on*, vol. 20, no. 3, pp. 1199–1206, Aug 2005.

[29] A. Brambilla, M. Gambarara, and G. Torrente, "Perturb and observe digital maximum power point tracker for satellite applications," in *Proc. of the Sixth European Conference, ESA*. Porto, Portugal: European Space Agency, May 2002, pp. 263–267.

[30] V. K. Ingle and J. G. Proakis, *Digital Signal Processing Using MATLAB*, 1st ed. Pacific Grove, CA, USA: Brooks/Cole Publishing Co., 1999.


**Federico Bizzarri** (M'12–SM'14) was born in Genoa, Italy, in 1974. He received the Laurea (M.Sc.) five-year degree (*summa cum laude*) in electronic engineering and the Ph.D. degree in electrical engineering from the University of Genoa, Genoa, Italy, in 1998 and 2001, respectively. Since October 2018 he has been an associate professor at the Electronic and Information Department of the Politecnico di Milano, Milan, Italy. He is a research fellow of the Advanced Research Center on Electronic Systems for Information and Communication Technologies "E. De Castro" (ARCES), University of Bologna, Italy. He served as an Associate Editor of the IEEE Transactions on Circuits and Systems — Part I from 2012 to 2015 and he was awarded as one of the 2012-2013 Best Associate Editors of this journal.

**Angelo Brambilla** (M'16) received the Dr. Ing. degree in electronics engineering from the University of Pavia, Pavia, Italy, in 1986. Currently he is full professor at the Dipartimento di Elettronica e Informazione, Politecnico di Milano, Milano, Italy, where he has been working in the areas of circuit analysis and simulation.